Cardiovascular homeostasis dependence on MICU2, a regulatory subunit of the mitochondrial calcium uniporter

Alexander G. Bick[a], Hiroko Wakimoto[a], Kimberli J. Kamer[b,c], Yasemin Sancak[b,c], Olga Goldberger[b,c], Anna Axelsson[a], Daniel M. DeLaughter[a], Joshua M. Gorham[a], Vamsi K. Mootha[b,c,d], J. G. Seidman[a], and Christine E. Seidman[a,d,e,1]

[a]Department of Genetics, Harvard Medical School, Boston, MA 02115; [b]Department of Molecular Biology, Massachusetts General Hospital, Boston, MA 02114; [c]Department of Systems Biology, Harvard Medical School, Boston, MA 02115; [d]Howard Hughes Medical Institute, Chevy Chase, MD 20815; and [e]Cardiovascular Division, Brigham and Women's Hospital, Boston, MA 02115

Contributed by Christine E. Seidman, September 8, 2017 (sent for review June 26, 2017; reviewed by Kenneth E. Bernstein and Elizabeth Murphy)

Comparative analyses of transcriptional profiles from humans and mice with cardiovascular pathologies revealed consistently elevated expression of *MICU2*, a regulatory subunit of the mitochondrial calcium uniporter complex. To determine if *MICU2* expression was cardioprotective, we produced and characterized *Micu2*$^{-/-}$ mice. Mutant mice had left atrial enlargement and *Micu2*$^{-/-}$ cardiomyocytes had delayed sarcomere relaxation and cytosolic calcium reuptake kinetics, indicating diastolic dysfunction. RNA sequencing (RNA-seq) of *Micu2*$^{-/-}$ ventricular tissues revealed markedly reduced transcripts encoding the apelin receptor (*Micu2*$^{-/-}$ vs. wild type, $P = 7.8 \times 10^{-40}$), which suppresses angiotensin II receptor signaling via allosteric transinhibition. We found that *Micu2*$^{-/-}$ and wild-type mice had comparable basal blood pressures and elevated responses to angiotensin II infusion, but that *Micu2*$^{-/-}$ mice exhibited systolic dysfunction and 30% lethality from abdominal aortic rupture. Aneurysms and rupture did not occur with norepinephrine-induced hypertension. Aortic tissue from *Micu2*$^{-/-}$ mice had increased expression of extracellular matrix remodeling genes, while single-cell RNA-seq analyses showed increased expression of genes related to reactive oxygen species, inflammation, and proliferation in fibroblast and smooth muscle cells. We concluded that *Micu2*$^{-/-}$ mice recapitulate features of diastolic heart disease and define previously unappreciated roles for *Micu2* in regulating angiotensin II-mediated hypertensive responses that are critical in protecting the abdominal aorta from injury.

mitochondrial calcium uniporter | diastolic dysfunction | aortic aneurysms | hypertension | calcium

The heart adapts to a variety of different stresses throughout life by adopting strategies to maintain excitation–contraction coupling and balance energy utilization and production. Genetic cardiomyopathies that cause ventricular hypertrophy (HCM) or dilatation (DCM) evoke chronic stress responses that have been identified in biochemical studies and transcriptional analyses of diseased cardiac tissues derived from human patients and model systems. Over a thousand genes with differential expression have been implicated in these responses, including molecules involved in cellular calcium flux (1–3).

Altered cardiac energetics is also a fundamental mechanistic component of HCM and DCM that is caused by mutations in sarcomere protein genes (4–8), and pharmacologic strategies are under study to correct energy deficits in patients with these disorders (9–11). Mutations in sarcomere proteins impact excitation–contraction coupling (12–15) and can alter cellular calcium flux, which in turn perturbs the balance of energy utilization and production in cardiomyocytes (16, 17). Changes in energy homeostasis can also reactivate fetal gene programs and promote profibrotic pathways and maladaptive remodeling that result in overt cardiomyopathy (18, 19).

Mutations that directly impact mitochondrial function also cause cardiomyopathies (20). These include mtDNA disorders such as MELAS (mitochondrial encephalomyopathy, lactic acidosis, and stroke-like episodes) and MERRF (myoclonic epilepsy with ragged-red fibers) (21). Likewise, cardiomyopathy occurs from mutations in nuclear-encoded mitochondrial genes that function in oxidative phosphorylation, including *TMEM70* [mitochondrial complex V ATP synthase deficiency (22)], *AGK* [Sengers or mitochondrial depletion syndrome (23)], and *AARS2* [infantile hypertrophic mitochondrial cardiomyopathy (24)]. In addition to heart disease, the abnormal mitochondrial responses in these disorders cause diabetes, neurological disease, vision loss, deafness (20), and, less commonly, aortic dilation (25) and rupture (26).

We hypothesized that key mediators of altered calcium homeostasis and energetics, processes in which mitochondria play central roles, might be consistently dysregulated across many cardiomyopathies. To identify these, we performed bioinformatic comparisons of cardiac transcriptional datasets from humans and mouse ventricular tissues with HCM or DCM. Among these, we identified one consistently dysregulated gene, *MICU2*, a calcium-sensing regulatory subunit of the mitochondrial calcium uniporter complex. Here we test the hypothesis that *MICU2* is a critical responder to cardiovascular stress. From studies of *Micu2*$^{-/-}$ mice, we report unexpected phenotypes that link mitochondrial calcium sensing and cardiovascular stress responses.

Significance

Hypertension increases the risk for development of abdominal aortic aneurysms, a silent pathology that is prone to rupture and cause sudden cardiac death. Male gender, smoking, and hypertension appear to increase risk for development of abdominal aortic aneurysms by provoking oxidative stress responses in cardiovascular tissues. Here we uncovered unexpected linkages between the calcium-sensing regulatory subunit MICU2 of the mitochondrial calcium uniporter and stress responses. We show that naive *Micu2*$^{-/-}$ mice had abnormalities of cardiac relaxation but, with modest blood pressure elevation, developed abdominal aortic aneurysms with spontaneous rupture. These findings implicate mitochondrial calcium homeostasis as a critical pathway involved in protecting cardiovascular tissues from oxidative stress.

Author contributions: A.G.B., V.K.M., and C.E.S. designed research; A.G.B., H.W., K.J.K., Y.S., O.G., A.A., D.M.D., and J.M.G. performed research; Y.S., O.G., A.A., and V.K.M. contributed new reagents/analytic tools; A.G.B., H.W., K.J.K., Y.S., D.M.D., V.K.M., J.G.S., and C.E.S. analyzed data; and A.G.B., Y.S., V.K.M., J.G.S., and C.E.S. wrote the paper.

Reviewers: K.E.B., Cedars-Sinai Medical Center; and E.M., NIH.

The authors declare no conflict of interest.

Freely available online through the PNAS open access option.

[1]To whom correspondence should be addressed. Email: cseidman@genetics.med.harvard.edu.

This article contains supporting information online at www.pnas.org/lookup/suppl/doi:10.1073/pnas.1711303114/-/DCSupplemental.

Results

We performed a bioinformatic screen to identify stress-responsive molecules in cardiomyopathy by intersecting differentially expressed genes from nine left ventricle (LV) transcriptome datasets: seven from human heart tissue from patients with HCM (*SI Appendix*, Table S1), and two from mouse models of HCM (*Myh6* p.R403Q) (1) and DCM (*Pln* p.R9C) (27). Approximately 300 genes were differentially expressed in both mouse cardiomyopathy datasets. Intersecting this list with the seven human transcriptomes identified only 6 genes that were consistently expressed in the same direction among all nine transcriptome profiles that could plausibly function in the stress response. Three of these genes participate in pathways involving cell growth and metabolism, including *IGFBP6* (insulin growth factor binding protein 6), *PRKAB2* (the beta-2 non-catalytic subunit of AMP-activated protein kinase), and *RHEB* (a small GTPase superfamily member that functions in insulin/TOR/S6K signaling). Another gene, *DAPK3* (expression of the death-associated protein kinase 3), participates in apoptosis pathways. Two mitochondrial proteins were also identified: *UCP2* (mitochondrial uncoupling protein), that encodes an inner-membrane transporter, and *MICU2* (mitochondrial calcium uptake 2), a regulatory subunit of the mitochondrial calcium uniporter complex that localizes to the mitochondrial intermembrane space, where it senses calcium levels to gate the activity of the mitochondrial calcium uniporter pore (28–31).

Recent studies link the mitochondrial calcium uniporter complex pore to both skeletal muscle and cardiac phenotypes. MCU is the uniporter's pore-forming subunit that, in combination with essential MCU regulator (EMRE), forms a functional channel in vivo (32, 33). Under basal conditions, MCU–EMRE is kept in the closed position by the calcium-sensing MICU1–MICU2 heterodimer that resides in the mitochondrial intermembrane space. In response to a threshold spike in calcium, the MICU1–MICU2 complex disinhibits the pore to allow calcium entry into mitochondria. Mice lacking *Mcu* exhibit impaired skeletal muscle metabolism and peak performance (34, 35). Similarly, in the heart, MCU participates in matching cardiac metabolism to contractile stress (36, 37) and also impacts heart rate (38). Although a global *Mcu* knockout mouse and cardiac-specific *Mcu* deficiency did not cause overt heart deficits at baseline or with isoproterenol infusion or transverse aortic constriction, rapid physiologic fight-or-flight responses were impaired (34–38). Moreover, mice expressing a dominant-negative *Mcu* had altered cardiac oxygen utilization, cytoplasmic Ca^{2+} homeostasis, and pathologic responses to ischemia-reperfusion injury (39).

These data prompted us to prioritize *MICU2* for further study. We hypothesized that if increased *MICU2* expression was cardioprotective, deletion of *MICU2* would promote cardiovascular dysfunction. To test this model, we generated a *Micu2*$^{-/-}$ mouse using a gene-trap vector (Fig. 1*A* and *SI Appendix*, Fig. S1*A*). *Micu2*$^{+/-}$ and *Micu2*$^{-/-}$ mice bred and produced offspring in Mendelian ratios, had comparable sizes and activity levels to wild-type littermates, and routinely lived for >18 mo. *Micu2*$^{+/-}$ mice had ∼50% normal levels of *Micu2* transcripts in hepatic, renal, and cardiac tissue. Transcript levels were further reduced in *Micu2*$^{-/-}$ mice (*SI Appendix*, Fig. S1*B*). We did not detect Micu2 protein in LV, aorta, or liver tissues from *Micu2*$^{-/-}$ mice by immunoblotting (Fig. 1 *B* and *C* and *SI Appendix*, Fig. S2). Consistent with prior results of RNAi targeting *Micu2* in mouse liver (28), both Micu1 and Mcu protein levels were significantly reduced in liver tissue from *Micu2*$^{-/-}$ mice (*SI Appendix*, Fig. S2*C*). We also confirmed prior studies that demonstrate that *Micu2*$^{-/-}$ mitochondria take up a high-concentration pulse of calcium more slowly than wild-type mitochondria (likely due to the reduction in Mcu levels) (28) but more rapidly take up lower-concentration pulses of calcium (*SI Appendix*, Fig. S3). These data are consistent with Micu2 setting the calcium threshold for the uniporter (30). Given these findings, we concluded that *Micu2*$^{-/-}$ mice had reduced levels of Micu2 protein and activity.

Cardiac structure and function of *Micu2*$^{-/-}$ mice were studied by histology, electron microscopy, and longitudinal echocardiography. Myocardial cellularity, cardiomyocyte size, and myocardial fibrosis in *Micu2*$^{-/-}$ and wild-type littermate mice were indistinguishable and sarcomere structure was normal (Fig. 1*D*). By contrast, electron microscopy revealed that in *Micu2*$^{-/-}$ mice (Fig. 1*E*), mitochondria were 20% smaller ($P = 0.003$) and 5% more eccentric ($P = 0.002$) than mitochondria from wild-type mice. Crista structure appeared normal.

Longitudinal echocardiography revealed that *Micu2*$^{-/-}$ mice had normal LV dimensions and fractional shortening (Table 1) but developed isolated left atrial (LA) enlargement at 16 to

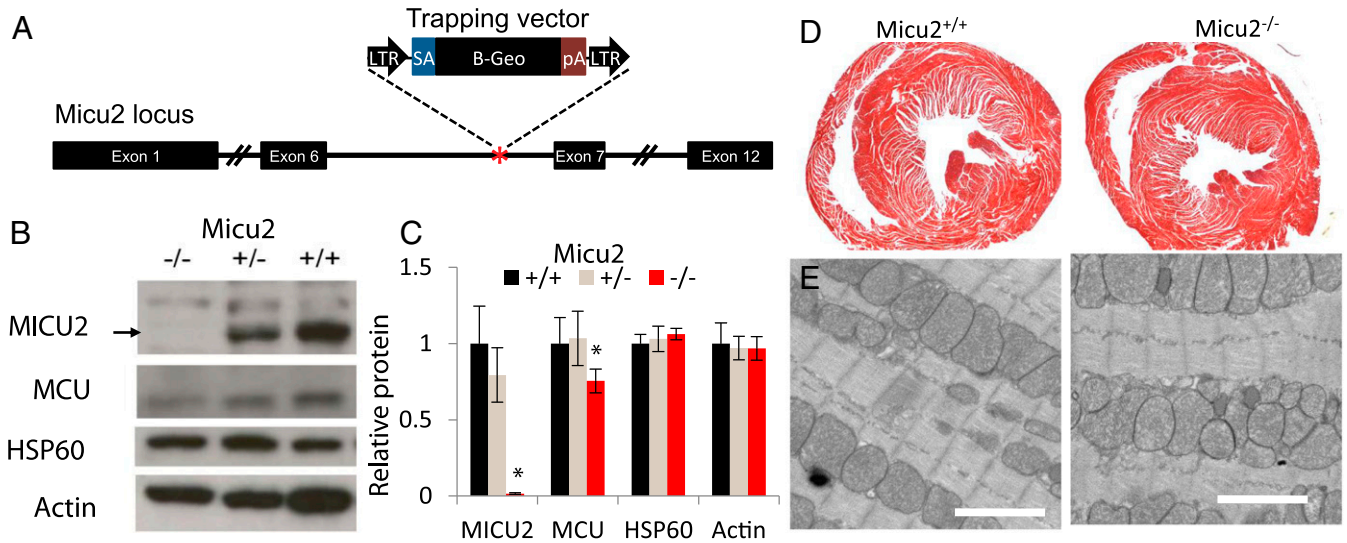

Fig. 1. Characterization of *Micu2*$^{-/-}$ mouse hearts. (*A*) Schema of the *Micu2* gene-trap vector used to generate the *Micu2*$^{-/-}$ mouse. (*B* and *C*) Protein levels of the mitochondrial calcium uniporter regulatory component Micu2 were significantly reduced in *Micu2*$^{-/-}$ mouse hearts. Protein expression of the uniporter pore calcium channel, Mcu, was 30% decreased. *$P < 0.05$. Error bars denote standard deviation. (*D*) Hearts of *Micu2*$^{-/-}$ mice were histologically indistinguishable from wild-type littermates. (*E*) Representative electron microscopy sections of *Micu2*$^{-/-}$ and wild-type mouse hearts. (Scale bars, 10 μm.)

Table 1. Echocardiographic assessment of cardiac structure and function in aged *Micu2*$^{-/-}$ mice

	WT (SD)	*Micu2*$^{-/-}$ (SD)	*P*
Left atrial diameter, mm	1.46 (0.06)	1.76 (0.08)	0.01
Intraventricular septum, mm	0.93 (0.02)	0.87 (0.03)	0.11
Posterior wall, mm	0.82 (0.04)	0.85 (0.02)	0.43
LV diameter, mm	3.32 (0.18)	3.48 (0.17)	0.53
Fractional shortening, %	49 (4.0)	48 (2.0)	0.97

Statistics are mean (SD). *P* values were calculated from a two-sided *t* test with five or six animals, age 15 to 18 mo, in each group.

18 mo of age (20% increased diameter, $P = 0.01$). LA enlargement can reflect the cumulative effect of increased diastolic LV pressure due to diastolic dysfunction (40, 41).

To better understand this diastolic dysfunction in mutant mice, we profiled sarcomere contractility and cytosolic calcium transients in single cardiomyocytes from three pairs of wild-type mice and *Micu2*$^{-/-}$ littermates (ages 6 to 8 wk). Although the extent and rate of contraction were comparable in *Micu2*$^{-/-}$ and wild-type cardiomyocytes, relaxation rates were slower ($P = 0.02$) in *Micu2*$^{-/-}$ cardiomyocytes (*SI Appendix*, Table S2). The magnitude of calcium flux in *Micu2*$^{-/-}$ and wild-type cardiomyocytes was similar; however, the time constant for calcium reuptake was increased ($P = 0.03$) in *Micu2*$^{-/-}$ cardiomyocytes (Fig. 2 and *SI Appendix*, Table S3). From these profiles, we deduced that slower reuptake of cytosolic calcium by *Micu2*$^{-/-}$ cardiomyocytes could retard relaxation and contribute to diastolic dysfunction.

Next, we analyzed the LV transcriptome in 18-wk-old *Micu2*$^{-/-}$ and wild-type mice by RNA sequencing (RNA-seq). Among the differentially expressed genes, the sarcoplasmic reticulum Ca^{2+}-ATPase (SERCA2a) encoded by *Atp2a* (Dataset S1; $P < 2 \times 10^{-260}$) was significantly increased, likely as a compensatory response for increased cytosolic calcium in *Micu2*$^{-/-}$ cardiomyocytes. Database for Annotation, Visualization, and Integrated Discovery (DAVID) gene set enrichment analyses of 700 differentially expressed genes identified several gene ontologies with significant dysregulation (Fig. 3 and Datasets S1 and S2), including sarcomere genes (5.9-fold, $P = 6 \times 10^{-8}$), bZIP transcription factors (8.1-fold, $P = 1.1 \times 10^{-8}$), stress response genes (7.1-fold, $P = 0.01$), and ribosomal proteins (8.4-fold, $P = 0.002$).

We partitioned differentially expressed genes into those primarily expressed in cardiomyocytes ($n = 64$) and nonmyocytes ($n = 89$) based on greater than fivefold difference in normalized transcript levels (42). Differentially expressed genes found in both compartments were excluded. Notably, cell-specific pathway analysis identified enrichment in sarcomere genes ($P = 2.5 \times 10^{-6}$) and oxidative phosphorylation ($P = 3.9 \times 10^{-4}$) in cardiomyocytes and bZIP transcription factors in nonmyocytes ($P = 2.9 \times 10^{-6}$). Among 1,100 genes that encode mitochondrial proteins (43, 44), only 46 genes were differentially expressed [odds ratio 1.1, P = NS (not significant)]. Two of the most significant changes in transcripts from *Micu2*$^{-/-}$ LV (Dataset S1) were a 1.6-fold decrease in the contractile protein gene *Myh7* ($P <$ 1e-50) and a 2.9-fold decrease in the apelin receptor (*Aplnr*; $P =$ 1e-40), findings that were independently confirmed by qPCR (Fig. 3*B*). Notably, two dysregulated bZIP proteins, ATF3 (activating transcription factor 3) and C/EBP-B (CCAAT/enhancer-binding protein-beta), regulate apelin expression in response to stress (45).

Given these transcriptional data, we hypothesized that *Micu2*$^{-/-}$ mice would be particularly sensitive to angiotensin II, since the apelin receptor suppresses angiotensin II type 1 receptor signaling via allosteric transinhibition (46, 47). As angiotensin II stimulates cardiac hypertrophy (48), we also expected that this provocation could increase diastolic dysfunction in *Micu2*$^{-/-}$ mice. Homozygous *Micu2*$^{-/-}$ mice, heterozygous *Micu2*$^{+/-}$ mice, and wild-type littermates were infused with 1.2 mg·kg^{-1}·d^{-1} of angiotensin II to increase systolic blood pressure over baseline by 25 mmHg ($P <$ 0.001; *SI Appendix*, Fig. S4). After 2 wk of treatment, all mice had equivalent increases in cardiac wall thickness, suggesting a comparable degree of hypertrophic remodeling (Table 2). However, *Micu2*$^{+/-}$ and *Micu2*$^{-/-}$ but not wild-type mice had significantly decreased fractional shortening in comparison with baseline ($P =$ 0.04 and $P = 0.002$, respectively).

Unexpectedly, 3 of 14 *Micu2*$^{-/-}$ but no wild-type mice died during angiotensin II infusion ($P = 0.03$; Fig. 4*A*). As autopsies revealed that all three had ruptured abdominal aortic aneurysms, we extended these studies to assess whether loss of *Micu2* impacted blood pressure and stress-induced vascular responses. Infusion of low (1.2 mg·kg^{-1}·d^{-1}) or high (2.4 mg·kg^{-1}·d^{-1}) doses of angiotensin II showed dose-dependent but equivalent increases in blood pressure in both *Micu2*$^{-/-}$ and wild-type mice (*SI Appendix*, Fig. S4).

Abdominal ultrasonography of untreated *Micu2*$^{-/-}$ mice ($n > 10$) showed slightly larger (5%) aortic artery diameters than wild-type mice ($P = 0.003$). Neither low nor high doses of angiotensin II infusion altered abdominal aortic diameters in wild-type mice, but *Micu2*$^{-/-}$ mice had dose-dependent increases in aortic diameters ($P = 0.0006$; Fig. 4*B*). Excluding mice with aortic rupture, a conservative estimate of the angiotensin II-induced aortic dilatation was at least 4.5-fold increased in *Micu2*$^{-/-}$ compared with wild-type mice.

Serial analyses of high-dose angiotensin II infusions revealed 10% increased abdominal aortic dimensions at day 2 in both *Micu2*$^{-/-}$ and wild-type mice. At day 4 and thereafter, aortic dimensions of wild-type mice remained unchanged while *Micu2*$^{-/-}$ mouse aortas continued to enlarge ($P = 0.005$; Fig. 4*C* and *SI Appendix*, Table S4).

To consider if this vascular pathology was blood pressure-mediated or angiotensin II-specific, we treated mice with norepinephrine (5.6 mg·kg^{-1}·d^{-1}). Using norepinephrine to increase blood pressures to equivalent levels induced by low-dose angiotensin II (*SI Appendix*, Fig. S4) did not induce aortic aneurysms in *Micu2*$^{-/-}$ or wild-type mice (Fig. 4*B*).

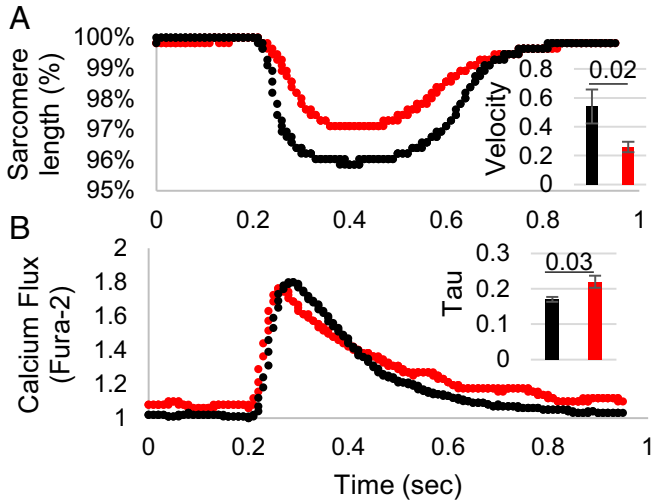

Fig. 2. Functional analysis of isolated *Micu2*$^{-/-}$ cardiomyocytes. Representative tracings of (*A*) single-myocyte sarcomere length (plotted as % of resting length) and (*B*) calcium flux (plotted as normalized Fura-2 intensity) in *Micu2*$^{-/-}$ mice and wild-type littermates. *Micu2*$^{-/-}$ cardiomyocytes had slower repolarization kinetics, as evidenced by both decreased sarcomere relaxation velocity (*A*, *Inset*) and increased time constant (Tau, the exponential decay of the ventricular pressure during isovolumic relaxation) for calcium reuptake (*B*, *Inset*) compared with wild-type cardiomyocytes (*Micu2*$^{-/-}$, $n = 22$ cells; wild type, $n = 31$ cells; *t* test). Error bars denote standard deviation.

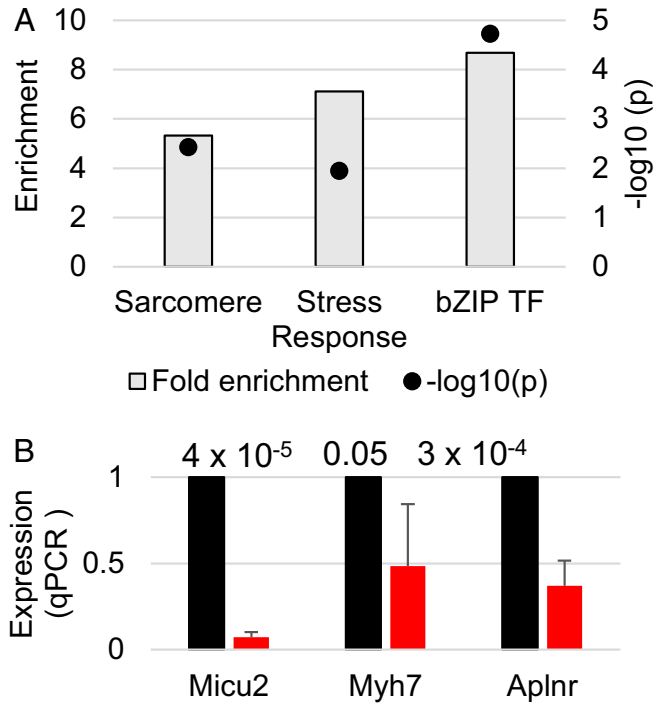

Fig. 3. Transcriptional analysis of *Micu2*$^{-/-}$ left ventricle. (*A*) Transcriptome-wide analysis of *Micu2*$^{-/-}$ and wild-type LV tissue (n = 3 mice) revealed enrichment in three gene sets: sarcomere components, stress response genes, and bZIP transcription factors (TF). Bonferroni-corrected P values are plotted. (*B*) *Micu2*, *Myh7*, and *Aplnr* were three of the most differentially expressed genes in the left ventricle RNA-seq datasets. Fold-change differences in these genes were independently confirmed with quantitative PCR (n = 5, t test). Mean and SD of *Micu2*$^{-/-}$ qPCR expression normalized to mean wild-type qPCR expression are plotted.

We studied vascular transcriptional response to *Micu2* deficiency by RNA-seq analyses of three aortas from 8- to 12-wk-old naive or angiotensin II-treated (1.2 mg/kg) *Micu2*$^{-/-}$ and wild-type littermates. Compared with wild type, untreated vascular tissues from *Micu2*$^{-/-}$ had significantly decreased (n = 478) and increased (n = 819) gene expression (Dataset S3). DAVID analyses identified 18 pathways from up-regulated genes and 23 pathways from down-regulated genes (Fig. 5*A* and Dataset S4). Among Bonferroni-corrected, significantly enriched gene sets with increased expression, we identified oxidation–reduction reaction genes (3.7-fold, $P = 6.2 \times 10^{-28}$), mitochondrial genes (2.8-fold, $P = 2.4 \times 10^{-35}$), and genes related to the peroxisome (7.0-fold, $P = 6.0 \times 10^{-13}$). Enrichments in down-regulated gene sets included myofibril (9.2-fold, $P = 1.6 \times 10^{-16}$), extracellular matrix (5.3-fold, $P = 6.59 \times 10^{-10}$), cell adhesion (3.4-fold, $P = 3.1 \times 10^{-12}$), blood vessel development (3.3-fold, $P = 0.01$), growth factor binding (6.2-fold, $P = 0.002$), and Wnt signaling (4.8-fold, $P = 0.002$). While we observed some overlap among the myofibril gene set and LV sarcomere genes, the majority of dysregulated genes in the heart and aorta were different, demonstrating tissue specificity in stress responses in *Micu2*$^{-/-}$ mice.

Analyses of the genes that were differentially expressed in the aorta only with angiotensin II treatment (180 genes increased; 603 genes decreased) showed enrichment in seven up-regulated pathways and nine down-regulated pathways (Datasets S5 and S6). Inflammatory-response genes (7-fold, $P = 8.7 \times 10^{-5}$) and extracellular matrix genes (7.2-fold, 3.2×10^{-9}) were significantly increased, while cell-junction genes (2.8-fold, $P = 4.4 \times 10^{-4}$) were significantly reduced.

Aneurysms arise from abnormalities of the intima, media, or adventitial layers of vascular beds that include fibroblast, smooth muscle, and endothelial cells. As histopathology of aortic aneurysms from *Micu2*$^{-/-}$ mice did not implicate a vascular layer or cell lineage (Fig. 4*A*, *Inset*), we attempted to deconvolute transcriptional changes by single-cell RNA-seq (49). From angiotensin II-treated *Micu2*$^{-/-}$ and wild-type aortas, we isolated 60 smooth muscle and fibroblast cells (*SI Appendix*, Fig. S6*A*) and 10 endothelial cells (likely due to smaller cell diameters that escaped microfluidic capture chips). The relative distribution of captured cell types was the same in *Micu2*$^{-/-}$ and wild-type aortas (P = NS).

Among aortic cells from wild-type mice, the distribution of *Micu2* expression did not differ by cell type (P = NS). *Micu2* was robustly expressed in 50% of endothelial, 23% of smooth muscle, and 18% of fibroblast cells, indicating that *Micu2* deficiency could affect each cell lineage.

Two patterns of altered gene expression were observed: differences in the absolute expression levels (quantitated by a Wilcox test on median differences; *SI Appendix*, Fig. S6*B*) and differences in the number of cells expressing an appreciable level of genes (quantitated with a Fisher test; *SI Appendix*, Fig. S6*C*). Too few endothelial cells were captured to identify genes exceeding the significance threshold (Bonferroni adjustment for significance was set at $P < 10^{-5}$ to reflect 5,000 expressed genes), but differential expression was identified in six smooth muscle cell genes and five fibroblast genes.

Among the six genes differentially expressed in *Micu2*$^{-/-}$ smooth muscle cells, we observed increased expression of genes associated with inflammation and reactive oxygen species (ROS) (*SI Appendix*, Fig. S6 *B* and *C*). Significantly more *Micu2*$^{-/-}$ (96%) than wild-type (29%) smooth muscle cells expressed extracellular glutathione peroxidase (*Gpx3*), the inflammatory cytokines *Tnfaip6* and *Ccl11*, and the transcription factor *Irf1*, which is associated with inflammation (50). Although the majority of *Micu2*$^{-/-}$ and wild-type smooth muscle cells expressed metallothionein (*Mt1*) that contributes to cardiovascular protection in high-ROS states (51), the median expression was ninefold higher in *Micu2*$^{-/-}$ smooth muscle cells ($P = 7.5 \times 10^{-8}$).

The five differentially expressed genes in *Micu2*$^{-/-}$ fibroblasts are involved in proliferation, inflammation, and ROS (*SI Appendix*, Figs. S6 *B* and *C*). More *Micu2*$^{-/-}$ fibroblasts (80%) than wild-type fibroblasts (10%) expressed the proproliferative transcription factor Myc ($P = 1.5 \times 10^{-6}$) (52). Most *Micu2*$^{-/-}$ (88%) but few wild-type (10%) fibroblasts expressed *Efemp1*, which induces EGFR autophosphorylation and activates cell adhesion and migration (9.6×10^{-8}) (53–55). *Micu2*$^{-/-}$ fibroblasts also showed significant differential gene expression of inflammatory and ROS genes, including decreased expression of *Fmo3* and *Sod3*, which reduce ROS free radicals (56, 57), and increased expression of the inflammatory mediator *Il6* (58).

Table 2. Cardiac structure and function in *Micu2*$^{-/-}$ mice after 2 wk of angiotensin II treatment

	WT (SD)	*Micu2*$^{-/-}$ (SD)	P
Systolic blood pressure, mmHg	141 (9.8)	142 (9.8)	0.94
Intraventricular septum, mm	0.89 (0.02)	0.82 (0.06)	0.28
Posterior wall, mm	0.82 (0.04)	0.82 (0.02)	0.93
LV diameter, mm	3.25 (0.11)	3.58 (0.15	0.09
Fractional shortening, %	36 (1.2)	28 (1.9)	0.006
Systolic strain, %	−19.3 (2.1)	−13.8 (2.5)	0.007

Statistics are mean (SD). P values were calculated from a two-sided t test with four to eight male mice, age 6 to 8 wk, in each group following 2 wk of angiotensin II infusion (1.2 mg·kg^{-1}·d^{-1}).

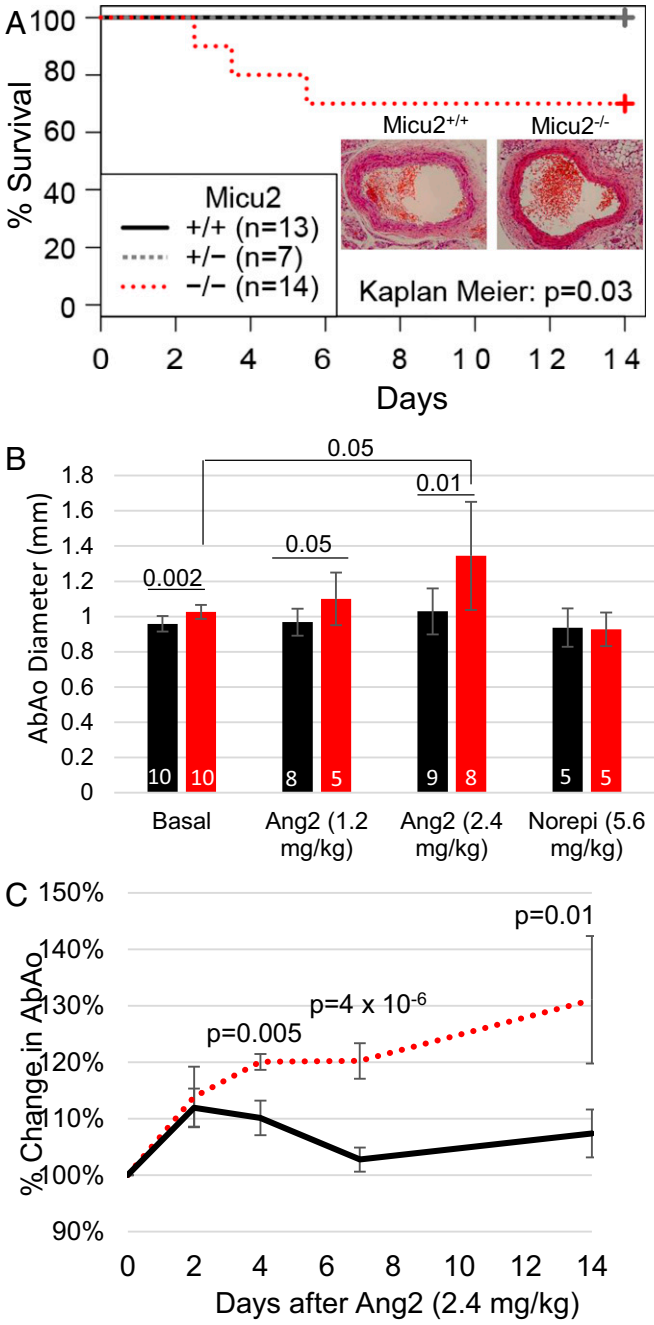

Fig. 4. *Micu2*$^{-/-}$ mice are susceptible to angiotensin II (Ang2)-induced aortic aneurysms. (*A*) In response to angiotensin II (1.2 mg/kg, $P = 0.03$) infusion, *Micu2*$^{-/-}$mice had abdominal aortic aneurysms and 30% of mice had lethal ruptures. (*A*, *Inset*) Representative abdominal aorta histological sections after 2 wk of angiotensin II infusion demonstrated grossly similar histologic patterns. Electron microscopy of *Micu2*$^{-/-}$ mouse aorta and liver showed no mitochondrial abnormalities (*SI Appendix*, Fig. S5). (*B*) Abdominal aortic (AbAo) diameter measured at baseline and 2 wk after angiotensin II infusion identified slightly enlarged diameters in *Micu2*$^{-/-}$ mice ($n > 10$) at baseline that was exaggerated with increasing angiotensin II dose (2.4 mg/kg). Aorta diameter did not change in response to norepinephrine. (*C*) Serial measurements of *Micu2*$^{-/-}$ and wild-type mice showed differential aortic enlargement by day 4 of angiotensin II infusion (2.4 mg/kg) ($n = 5$ mice, *t* test at each time point). Bars indicate standard deviation.

Discussion

Our data establish a critical role for *Micu2*, and presumably the mitochondrial calcium uniporter channel complex, in maintaining cardiovascular homeostasis in health and disease. Loss of *Micu2* produced cardiac diastolic dysfunction with LA enlargement, abnormalities that are likely secondary to delayed calcium reuptake and decreased relaxation rates by cardiomyocytes. *Micu2* depletion did not significantly alter gene expression of *Mcu* or *Micu1*, but protein levels of both were reduced. Hence, the cellular consequences of *Micu2* loss are attributable to the combination of two effects: (*i*) a decrease in the threshold for mitochondrial calcium uptake due to loss of the gatekeeping activity of Micu2; and (*ii*) overall loss of mitochondrial calcium uptake by the uniporter due to destabilization of Mcu and the entire complex. Moreover, changes in protein levels of Mcu and Micu1 after genetic ablation of *Micu2* indicate that homeostatic interactions among components of the mitochondrial calcium uniporter complex may be important for stability. The resultant altered calcium dynamics was associated with pathologic transcriptional signatures in cardiomyocytes and nonmyocytes. Gene expression in *Micu2*$^{-/-}$ hearts was characterized by sarcomere dysregulation, stress response pathways, and altered expression of sarcomere genes and the bZIP family of transcription factors, molecules that contribute to cardiomyopathy pathogenesis and that regulate apelin signaling (2, 3, 59, 60).

In the setting of cardiovascular disease, *Micu2* expression was particularly important. Hypertensive *Micu2*$^{-/-}$ mice had both diastolic and systolic dysfunction, as evidenced by decreased fractional shortening and altered systolic strain measurements. Despite these functional abnormalities, LV dimensions in *Micu2*$^{-/-}$ mice remained normal. As such, hypertensive *Micu2*$^{-/-}$ mice may provide a first step toward the development of an animal model for heart failure with preserved ejection fraction, a prevalent and poorly understood human disease (61).

The molecular mechanisms for diastolic dysfunction are incompletely understood. At the cellular level, cardiomyocyte relaxation requires tightly bound actin–myosin filaments to detach, a process mediated in part by calcium removal. Reduced or delayed calcium reuptake into the sarcoplasmic reticulum (SR) or mitochondria or removal from cardiomyocytes can delay relaxation (62). In addition, abnormal mitochondrial calcium homeostasis can influence NADPH levels and the redox state of cardiomyocytes to perturb relaxation. Consistent with these observations, malfunction of multiple calcium-handling proteins propel heart failure, including SERCA2a and its modulator phospholamban (PLB), the SR–Ca^{2+} release channel and its modulator FK-506 binding protein 12.6 (FKBP12.6), and the sodium–calcium exchanger (63–66). We suggest that Micu2 contributes to restoration of diastolic calcium levels by sensing cytosolic levels and dynamically gating calcium uptake of the mitochondrial calcium uniporter, similar to activities of PLB or FKBP12.6 proteins. Consistent with this model, we note that hepatocyte mitochondria from *Micu2*$^{-/-}$ mice, which lack multiple calcium-buffering mechanisms, uptake high concentrations of calcium significantly more slowly than wild-type mitochondria (28), likely due to destabilization of the entire channel complex. While cardiomyocytes have multiple pathways to remove high concentrations of calcium that occur with each contraction, fine-tuning by mitochondrial calcium uptake may also be important in cardiac calcium dynamics and could account for the decreased cytosolic calcium reuptake that we observed in *Micu2*$^{-/-}$ cardiomyocytes.

Several recent studies have probed how changes in components of the mitochondrial calcium uniporter complex regulate and integrate mitochondrial and cellular calcium homeostasis (29, 67). *Micu2*-null mice on an isogenic C57/B6 background are viable and have minimal basal abnormalities, whereas *Micu1*-null mice on an isogenic C57/B6 background exhibit perinatal mortality due to mitochondrial calcium overload (68, 69). A challenge in interpreting the consequences of genetic loss of one of these subunits is that they can cross-stabilize each other in a tissue-specific manner. The consensus in the field is that Micu1 functions as an essential gatekeeper that regulates calcium influx into the mitochondria (70). The inhibitory activity of

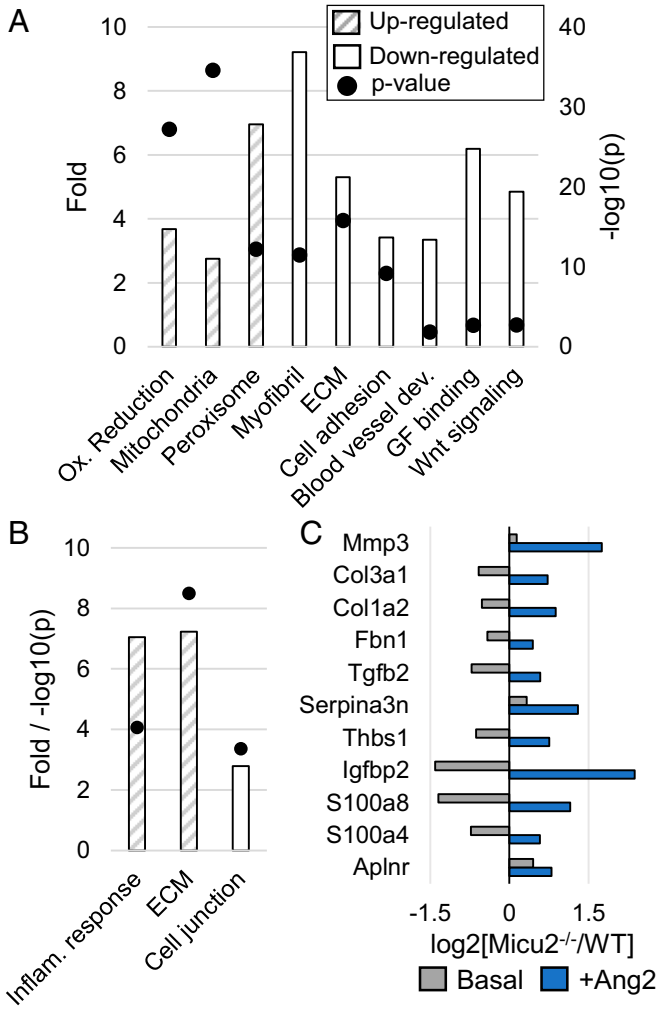

Fig. 5. Transcriptional dissection of *Micu2*$^{-/-}$ aortic aneurysm. (*A*) RNA-seq and pathway enrichment analyses of untreated *Micu2*$^{-/-}$ mice ($n = 3$) compared with wild-type mice ($n = 3$) identified gene sets with increased (shaded bars) and decreased (clear bars) expression. GF, growth factor. Bonferroni-corrected *P* values are shown. (*B*) RNA-seq pathway enrichment analysis of mouse aorta tissue after angiotensin II infusion (1.2 mg/kg for 2 wk) identified three notable changes in gene sets. (*C*) Fold change of selected genes with known roles in aneurysm formation after angiotensin II (1.2 mg/kg) versus basal state with significant differential expression by RNA-seq.

Micu2 is dependent on its physical association with Micu1. At low calcium concentrations, heterodimers between Micu1 and Micu2 negatively regulate calcium import by Mcu, while at high calcium concentrations, the Micu1–Micu2 inhibition is relieved and calcium uptake occurs (31). Oxidative stress imposes further modification of a cysteine residue in Mcu that results in conformational changes of the pore-forming unit and persistent mitochondrial uptake of calcium (71). Responses to changes in the mitochondrial calcium uniporter complex further impact calcium homeostasis. For example, marked depletion (80%) of *Mcu* expression in cardiomyocytes reduces the activity and expression of the mitochondrial sodium–calcium exchanger, so as to maintain normal cytosolic calcium (36). By contrast, cytosolic calcium is increased in cardiomyocytes that chronically express a dominant-negative *Mcu* construct (39) or, as described here, lack the pore's inhibitory subunit Micu2, without changes in the expression of the mitochondrial sodium–calcium exchanger but with increased SERCA2a activity (39) or expression (Dataset S1). Collectively, these data point to the multiple integrated mitochondrial and cytosolic strategies to maintain calcium homeostasis in cardiomyocytes and other cells.

Our studies uncovered unexpected and critical roles for physiologic regulation of the mitochondrial calcium uniporter complex to maintain calcium homeostasis in vascular tissues. In the setting of angiotensin II-induced hypertension, *Micu2*$^{-/-}$ mice were prone to lethal abdominal aortic aneurysms. Transcriptional profiles of the *Micu2*$^{-/-}$ aorta implicated molecules and pathways known to promote aneurysm formation, including the proinflammatory state, increased extracellular matrix remodeling, and cellular proliferation (72–76). Matrix metalloproteinase 3 (*Mmp3*), which degrades collagen, fibronectin, laminin, and elastin, had significantly increased expression (77). *Mmp3* gene polymorphisms are associated with aneurysm formation in human patients (78, 79), and deletion of *Mmp3* in mice reduces aneurysm formation (74). The expression of *Col3a1* and *Col1a2*, molecules that cause vascular disease in Ehlers–Danlos syndrome (80–82), were increased in angiotensin II-treated *Micu2*$^{-/-}$ mice, a finding suggestive of active collagen degradation from increased *Mmp3* expression. Angiotensin II increased the expression of other genes implicated in human aneurysms, most notably *Fbn1* (fibrillin-1, mutated in Marfan syndrome) and *TGFβ2* (transforming growth factor beta-2, mutated in Loeys–Dietz syndrome) (83–85).

Two calgranulins, *S100a8* and *S100a4*, that were decreased in untreated *Micu2*$^{-/-}$ mice and increased after angiotensin II infusion are well-positioned to directly link altered calcium flux to aneurysm. Calgranulins are a family of small acidic calcium signaling proteins that promote inflammation and vascular disease by activating the receptor for advanced glycation end products (RAGE) (86), and are linked to vascular dysfunction and atherosclerosis (87, 88). *S100a4* is strongly up-regulated in human thoracic aortic aneurysms (89) and intracranial aneurysms (90). Mechanistically, silencing *S100a4* decreases vascular smooth proliferation and matrix metalloproteinase expression (89).

Notably, *Micu2*$^{-/-}$ mice did not develop aneurysms in the setting of norepinephrine-induced hypertension, a finding that implicates angiotensin II-specific signaling. Angiotensin II has been shown to activate noncanonical TGFβ signaling (ERK1/2) via protein kinase C (83–85, 91–93). Recent studies of *Fbn1*$^{-/-}$ mice (modeling Marfan syndrome) treated with calcium channel blockers had accelerated thoracic aortic aneurysm expansion and rupture through a protein kinase C-mediated pathway, further implicating cross-talk between calcium signaling, TGFβ, and aneurysms (94). Clinical evidence also supports the link between calcium and aneurysm formation. A retrospective study of human patients identified the use of calcium channel blockers as an independent risk factor for abdominal aortic aneurysms (95). These data and our findings motivate further investigations into mitochondrial calcium homeostasis and aneurysm formation.

Angiotensin II and loss of the *Micu2* paralog and binding partner *Micu1* can trigger oxidative stress and vascular dysfunction (96, 97). These data, combined with our transcriptional analyses, implicate oxidative stress in the pathogenesis of aneurysm in angiotensin II-treated *Micu2*$^{-/-}$ mice. While atherogenic mice are thought to develop abdominal aortic aneurysms via reactive oxygen species (98, 99), the *Micu2*$^{-/-}$ mice described here implicate abnormal mitochondrial calcium handling. It is notable that these two pathways, oxidative stress and mitochondrial calcium transport by the uniporter, have recently been mechanistically linked at a molecular level (71, 100). Further elucidation of the mitochondrial molecules and pathways that impact stress-induced calcium signaling are expected to further insights into disease pathogenesis and perhaps uncover novel therapeutic strategies to treat abdominal aortic aneurysms.

Materials and Methods

The *Micu2* mice were derived from the gene-trap allele (*Micu2*; OST409343) that was generated by the Texas A&M Institute for Genomic Medicine. The

Victr 37 viral plasmid was used to insert a splice acceptor, β-geo (β-galactosidase/neomycin) cassette, synthetic polyA signal/transcriptional blocker, and PGK promoter/BTK exon/splice donor cassette, all flanked by two viral long-terminal repeat segments in-between exons 4 and 5 of the *Micu2* locus. Mice were derived and backcrossed onto the C57/B6 background for >10 generations. All animal experiments and procedures were reviewed and approved by the Institutional Animal Care and Use Committee at Harvard Medical School.

Immunoblots. Immunoblots were performed using antibodies from Sigma (Micu1, Mcu, actin), Abcam (HSP60, ATP5a), and BD Biosciences (TIMM23). Antibodies against Micu2 and EMRE were produced in collaboration with Bethyl.

Mouse Liver Mitochondrial Isolation and Calcium Uptake Analysis. Mitochondria were isolated from mouse liver using differential centrifugation as previously described (28) and resuspended in 220 mM mannitol, 75 mM sucrose, 10 mM Hepes (pH 7.4), 1 mM EDTA, and 0.2% BSA and kept on ice. Calcium uptake assays were performed by adding 120 μg mitochondria to 150 μL buffer containing 125 mM KCl, 2 mM K_2HPO_4, 1 mM $MgCl_2$, 20 mM Hepes at pH 7.2, 5 mM glutamate and malate, and 1 μM Oregon Green-Bapta6F. Fluorescence was monitored using a PerkinElmer EnVision plate reader in response to various pulses of $CaCl_2$. The relative rate of calcium uptake is reported using a linear fit of fluorescence from 30 to 40 s ($n = 3$).

Mouse Echocardiography and Abdominal Ultrasonography. Mice were anesthetized with an isoflurane vaporizer (VetEquip), and each limb was placed on ECG leads on a Vevo Mouse Handling Table (VisualSonics), maintaining the body temperature at 37 °C during the study. Transthoracic echocardiography and transabdominal ultrasonography were performed using the Vevo 2100 High-Resolution In Vivo Micro-Imaging System and MS550D transducer (VisualSonics), with heart rate at 500 to 550 beats per min. The images were acquired as 2D (left parasternal long and short axes), M-mode (left parasternal short axis), speckle tracking, and transabdominal 2D measurements. Measurements were averaged from images acquired during three consecutive heart beats. All echocardiogram and sonogram measurements were performed with an experienced operator blinded to mouse genotype. Differences between groups of mice were determined using the unpaired Student's *t* test.

Single-Cardiomyocyte Functional Profiling. Ventricular cardiomyocytes from three pairs of adult wild-type and *Micu2*$^{-/-}$ littermates at 6 to 8 wk of age, on 3 separate days, were isolated via a Langendorff-perfused heart preparation using enzymatic digestion as previously described (101). After isolation, the cells were suspended in Tyrode's buffer with gradually increasing Ca^{2+} concentrations (0.06, 0.6, and 1.2 mM, pH 7.4 at room temperature) and loaded with 1 μM Fura-2 AM calcium indicator (Molecular Probes) as previously described (102). Myocytes were washed three times for 10 to 15 min with 1.2 mM Ca^{2+} Tyrode's solution containing 250 μM probenecid to retain the indicator in the cytosol. The experiments were then performed at room temperature in 1.2 mM Ca^{2+} Tyrode's solution containing 140 mM NaCl, 4.5 mM KCl, 0.5 mM $MgCl_2$, 5 mM glucose, and 10 mM Hepes, pH adjusted to 7.4 with NaOH.

Cardiomyocytes were electrically paced at 60 beats per min via platinum wires. Sarcomere shortening/relengthening and Fura-2 fluorescence ratios (which reflect the intracellular calcium transients) were simultaneously recorded and determined from discrete striation positions on the myocyte using a dual-excitation fluorescence imaging/contractility recording system (IonWizard SarcLen detection and PMT acquisition fluorescence system; IonOptix). Sarcomere length and Ca^{2+} transients were analyzed using IonOptix transient analysis software. Myocytes included in the study were rod-shaped with a clear striation pattern, quiescent in the absence of electrical stimulation, and with a resting sarcomere length of more than 1.6 μm. At least seven myocytes were profiled from each animal. Statistical analysis was performed with a two-sample, one-tailed Student's *t* test.

Electron Microscopy. LV tissue from three pairs of wild-type and *Micu2*$^{-/-}$ littermates at 18 wk of age were evaluated in a blinded fashion with seven representative fields per mouse imaged at 1,900× resolution on a Tecnai G2 Spirit BioTWIN transmission electron microscope (FEI). The average mitochondrial size and eccentricity were automatically quantitated with CellProfiler (Broad Institute).

Pharmacologic Manipulation with Angiotensin II. Hypertension was induced in mice by chronic infusion with angiotensin II (Sigma-Aldrich) dissolved in saline at 1.4 $mg \cdot kg^{-1} \cdot d^{-1}$ or 2.8 $mg \cdot kg^{-1} \cdot d^{-1}$ or norepinephrine dissolved in saline at 5.6 $mg \cdot kg^{-1} \cdot d^{-1}$, via an osmotic minipump for 2 wk (103).

Blood Pressure Measurement. Systolic blood pressure was measured in trained conscious mice, maintained at normal body temperature, using a BP-2000 Analysis System (Visitech Systems) as previously described (104). Mice were "trained" to the procedure twice daily for 3 consecutive days, and data were recorded over the following 2 d. Statistical analyses are from 10 readings for each mouse.

Transcriptome-Wide Analyses. Human tissue samples from HCM patients were obtained from study participants undergoing either myectomy heart surgery, cardiac transplant surgery, or valve replacement surgery with informed consent, using IRB-approved protocols at Brigham and Women's Hospital.

RNA from human tissues and mouse LV was prepared and RNA-seq libraries were constructed as previously described (105). Uniform amplification of the cDNA library was achieved with amplification cycling before the reaction reached saturation, as determined by quantitative PCR. Aorta RNA-seq libraries were constructed with the Nextera library preparation method (106). To reduce biological variation in mouse specimens, RNA was pooled from three biological replicates for LV samples and angiotensin II-treated aorta samples. For the basal aorta RNA-seq samples, libraries from three biological replicates for each genotype (*Micu2*$^{-/-}$ and wild type) were constructed and the libraries were sequenced individually.

Libraries were sequenced on an Illumina HiSeq 2000 sequencer with 50-bp paired-end reads. Following sequencing, alignment of reads to the mm10 genome was performed with Bowtie and TopHat (107). Gene expression profiles were constructed by tallying reads on gene loci, using a Bayesian *P* value to assess the significance of gene expression differences between pooled samples (108). Cuffdiff 2 was used for assessing the significance of gene expression differences in aorta RNA-seq library replicates (109).

Genes were considered differentially expressed if there was a >40% increase or decrease in fold change with $P < 10^{-3}$. The DCM mouse model and HCM mouse model transcriptome datasets were previously described (110, 111). Gene ontology pathway enrichment analysis was performed with DAVID (112).

Single-Cell RNA-Seq. Mouse aortas were dissected and digested into single cells using collagenase. Cells were captured, and RNA was extracted and amplified into cDNA libraries using the Fluidigm C1 system as previously described (113). Libraries were sequenced on an Illumina HiSeq 2000 sequencer with 50-bp paired-end reads. Reads were aligned using TopHat. The expression of known markers for vascular lineages was used to classify each cell as a smooth muscle cell (*Acta2*, *Tagln*, *Myh11*), fibroblast (*Vim*), or endothelial cell (*Pecam1*, *Tek*, *Cdh5*). Cells lacking any of these markers were classified as "undetermined." Wilcox and Fisher test *P* values were calculated in the R statistical computing environment, version 2.15 (www.r-project.org).

ACKNOWLEDGMENTS. We thank Dr. Richard Mitchell for helpful discussions. A.G.B. was supported by NIH Graduate Fellowship T32GM007753. K.J.K. was supported by a graduate research fellowship from the National Science Foundation. Y.S. received support from the Helen Hay Whitney Foundation. This work was supported by a gift from W. Dan and Pat Wright (to V.K.M.) and grants from Fondation Leducq (to J.G.S. and C.E.S.) and the Howard Hughes Medical Institute (to V.K.M. and C.E.S.).

1. Geisterfer-Lowrance AA, et al. (1996) A mouse model of familial hypertrophic cardiomyopathy. *Science* 272:731–734.
2. Konno T, Chang S, Seidman JG, Seidman CE (2010) Genetics of hypertrophic cardiomyopathy. *Curr Opin Cardiol* 25:205–209.
3. Teekakirikul P, Padera RF, Seidman JG, Seidman CE (2012) Hypertrophic cardiomyopathy: Translating cellular cross talk into therapeutics. *J Cell Biol* 199:417–421.
4. Güçlü A, et al. (2013) ENerGetIcs in hypertrophic cardiomyopathy: TraNslation between MRI, PET and cardiac myofilament function (ENGINE study). *Neth Heart J* 21:567–571.
5. Ingwall JS (2004) Transgenesis and cardiac energetics: New insights into cardiac metabolism. *J Mol Cell Cardiol* 37:613–623.
6. Maack C, O'Rourke B (2007) Excitation-contraction coupling and mitochondrial energetics. *Basic Res Cardiol* 102:369–392.
7. Sulakhe PV, Dhalia NS (1971) Excitation-contraction coupling in heart. VII. Calcium accumulation in subcellular particles in congestive heart failure. *J Clin Invest* 50:1019–1027.
8. Tardiff JC, et al. (2015) Targets for therapy in sarcomeric cardiomyopathies. *Cardiovasc Res* 105:457–470.
9. Abozguia K, et al. (2010) Metabolic modulator perhexiline corrects energy deficiency and improves exercise capacity in symptomatic hypertrophic cardiomyopathy. *Circulation* 122:1562–1569.
10. Beadle RM, et al. (2015) Improvement in cardiac energetics by perhexiline in heart failure due to dilated cardiomyopathy. *JACC Heart Fail* 3:202–211.

11. Dass S, et al. (2015) Exacerbation of cardiac energetic impairment during exercise in hypertrophic cardiomyopathy: A potential mechanism for diastolic dysfunction. *Eur Heart J* 36:1547–1554.
12. Gao WD, Pérez NG, Seidman CE, Seidman JG, Marbán E (1999) Altered cardiac excitation-contraction coupling in mutant mice with familial hypertrophic cardiomyopathy. *J Clin Invest* 103:661–666.
13. Hasenfuss G, et al. (1992) Alteration of contractile function and excitation-contraction coupling in dilated cardiomyopathy. *Circ Res* 70:1225–1232.
14. Palmer BM, et al. (2004) Differential cross-bridge kinetics of FHC myosin mutations R403Q and R453C in heterozygous mouse myocardium. *Am J Physiol Heart Circ Physiol* 287:H91–H99.
15. Palmer BM, et al. (2013) Elevated rates of force development and MgATP binding in F764L and S532P myosin mutations causing dilated cardiomyopathy. *J Mol Cell Cardiol* 57:23–31.
16. Taegtmeyer H, King LM, Jones BE (1998) Energy substrate metabolism, myocardial ischemia, and targets for pharmacotherapy. *Am J Cardiol* 82(Suppl 1):54K–60K.
17. Territo PR, Mootha VK, French SA, Balaban RS (2000) Ca(2+) activation of heart mitochondrial oxidative phosphorylation: Role of the F(0)/F(1)-ATPase. *Am J Physiol Cell Physiol* 278:C423–C435.
18. Depre C, Davies PJA, Taegtmeyer H (1999) Transcriptional adaptation of the heart to mechanical unloading. *Am J Cardiol* 83(Suppl 1):58H–63H.
19. Teekakirikul P, et al. (2010) Cardiac fibrosis in mice with hypertrophic cardiomyopathy is mediated by non-myocyte proliferation and requires Tgf-β. *J Clin Invest* 120: 3520–3529.
20. Koopman WJH, Willems PHGM, Smeitink JAM (2012) Monogenic mitochondrial disorders. *N Engl J Med* 366:1132–1141.
21. Lieber DS, et al. (2013) Targeted exome sequencing of suspected mitochondrial disorders. *Neurology* 80:1762–1770.
22. Calvo S, et al. (2006) Systematic identification of human mitochondrial disease genes through integrative genomics. *Nat Genet* 38:576–582.
23. Calvo SE, et al. (2012) Molecular diagnosis of infantile mitochondrial disease with targeted next-generation sequencing. *Sci Transl Med* 4:118ra10.
24. Götz A, et al. (2011) Exome sequencing identifies mitochondrial alanyl-tRNA synthetase mutations in infantile mitochondrial cardiomyopathy. *Am J Hum Genet* 88: 635–642.
25. Brunetti-Pierri N, et al. (2011) Dilation of the aortic root in mitochondrial disease patients. *Mol Genet Metab* 103:167–170.
26. Tay SH, et al. (2006) Aortic rupture in mitochondrial encephalopathy, lactic acidosis, and stroke-like episodes. *Arch Neurol* 63:281–283.
27. Schmitt JP, et al. (2003) Dilated cardiomyopathy and heart failure caused by a mutation in phospholamban. *Science* 299:1410–1413.
28. Plovanich M, et al. (2013) MICU2, a paralog of MICU1, resides within the mitochondrial uniporter complex to regulate calcium handling. *PLoS One* 8:e55785.
29. Kamer KJ, Mootha VK (2015) The molecular era of the mitochondrial calcium uniporter. *Nat Rev Mol Cell Biol* 16:545–553.
30. Kamer KJ, Mootha VK (2014) MICU1 and MICU2 play nonredundant roles in the regulation of the mitochondrial calcium uniporter. *EMBO Rep* 15:299–307.
31. Kamer KJ, Grabarek Z, Mootha VK (2017) High-affinity cooperative Ca^{2+} binding by MICU1–MICU2 serves as an on–off switch for the uniporter. *EMBO Rep* 18: 1397–1411.
32. Sancak Y, et al. (2013) EMRE is an essential component of the mitochondrial calcium uniporter complex. *Science* 342:1379–1382.
33. Kovács-Bogdán E, et al. (2014) Reconstitution of the mitochondrial calcium uniporter in yeast. *Proc Natl Acad Sci USA* 111:8985–8990.
34. Holmström KM, et al. (2015) Assessment of cardiac function in mice lacking the mitochondrial calcium uniporter. *J Mol Cell Cardiol* 85:178–182.
35. Pan X, et al. (2013) The physiological role of mitochondrial calcium revealed by mice lacking the mitochondrial calcium uniporter. *Nat Cell Biol* 15:1464–1472.
36. Kwong JQ, et al. (2015) The mitochondrial calcium uniporter selectively matches metabolic output to acute contractile stress in the heart. *Cell Rep* 12:15–22.
37. Luongo TS, et al. (2015) The mitochondrial calcium uniporter matches energetic supply with cardiac workload during stress and modulates permeability transition. *Cell Rep* 12:23–34.
38. Wu Y, et al. (2015) The mitochondrial uniporter controls fight or flight heart rate increases. *Nat Commun* 6:6081.
39. Rasmussen TP, et al. (2015) Inhibition of MCU forces extramitochondrial adaptations governing physiological and pathological stress responses in heart. *Proc Natl Acad Sci USA* 112:9129–9134.
40. Nagueh SF, et al. (2009) Recommendations for the evaluation of left ventricular diastolic function by echocardiography. *J Am Soc Echocardiogr* 22:107–133.
41. Tsang TS, Barnes ME, Gersh BJ, Bailey KR, Seward JB (2002) Left atrial volume as a morphophysiologic expression of left ventricular diastolic dysfunction and relation to cardiovascular risk burden. *Am J Cardiol* 90:1284–1289.
42. Burke MA, et al. (2016) Molecular profiling of dilated cardiomyopathy that progresses to heart failure. *JCI Insight* 1:e86898.
43. Foster LJ, et al. (2006) A mammalian organelle map by protein correlation profiling. *Cell* 125:187–199.
44. Pagliarini DJ, et al. (2008) A mitochondrial protein compendium elucidates complex I disease biology. *Cell* 134:112–123.
45. Jeong K, et al. (2014) Apelin is transcriptionally regulated by ER stress-induced ATF4 expression via a p38 MAPK-dependent pathway. *Apoptosis* 19:1399–1410.
46. Siddiquee K, Hampton J, McAnally D, May L, Smith L (2013) The apelin receptor inhibits the angiotensin II type 1 receptor via allosteric trans-inhibition. *Br J Pharmacol* 168:1104–1117.
47. Sun X, et al. (2011) Non-activated APJ suppresses the angiotensin II type 1 receptor, whereas apelin-activated APJ acts conversely. *Hypertens Res* 34:701–706.
48. Crowley SD, et al. (2006) Angiotensin II causes hypertension and cardiac hypertrophy through its receptors in the kidney. *Proc Natl Acad Sci USA* 103:17985–17990.
49. Islam S, et al. (2014) Quantitative single-cell RNA-seq with unique molecular identifiers. *Nat Methods* 11:163–166.
50. Bachmaier K, et al. (1997) iNOS expression and nitrotyrosine formation in the myocardium in response to inflammation is controlled by the interferon regulatory transcription factor 1. *Circulation* 96:585–591.
51. Cai L, et al. (2006) Attenuation by metallothionein of early cardiac cell death via suppression of mitochondrial oxidative stress results in a prevention of diabetic cardiomyopathy. *J Am Coll Cardiol* 48:1688–1697.
52. Yao Y, et al. (2014) PIWIL2 induces c-Myc expression by interacting with NME2 and regulates c-Myc-mediated tumor cell proliferation. *Oncotarget* 5:8466–8477.
53. Song EL, et al. (2011) EFEMP1 expression promotes angiogenesis and accelerates the growth of cervical cancer in vivo. *Gynecol Oncol* 121:174–180.
54. Sukhatme VP, et al. (1988) A zinc finger-encoding gene coregulated with c-fos during growth and differentiation, and after cellular depolarization. *Cell* 53:37–43.
55. Zeng XR, Sun Y, Wenger L, Cheung HS (2005) Basic calcium phosphate crystal-induced Egr-1 expression stimulates mitogenesis in human fibroblasts. *Biochem Biophys Res Commun* 330:658–664.
56. Stadtman ER, Moskovitz J, Berlett BS, Levine RL (2002) Cyclic oxidation and reduction of protein methionine residues is an important antioxidant mechanism. *Mol Cell Biochem* 234–235:3–9.
57. Zhang X, et al. (2012) MicroRNA-21 modulates the levels of reactive oxygen species by targeting SOD3 and TNFα. *Cancer Res* 72:4707–4713.
58. Matsusaka T, et al. (1993) Transcription factors NF-IL6 and NF-kappa B synergistically activate transcription of the inflammatory cytokines, interleukin 6 and interleukin 8. *Proc Natl Acad Sci USA* 90:10193–10197.
59. Fentzke RC, Korcarz CE, Lang RM, Lin H, Leiden JM (1998) Dilated cardiomyopathy in transgenic mice expressing a dominant-negative CREB transcription factor in the heart. *J Clin Invest* 101:2415–2426.
60. Huggins GS, et al. (2007) The CREB leucine zipper regulates CREB phosphorylation, cardiomyopathy, and lethality in a transgenic model of heart failure. *Am J Physiol Heart Circ Physiol* 293:H1877–H1882.
61. Gaasch WH, Zile MR (2004) Left ventricular diastolic dysfunction and diastolic heart failure. *Annu Rev Med* 55:373–394.
62. Kass DA, Bronzwaer JG, Paulus WJ (2004) What mechanisms underlie diastolic dysfunction in heart failure? *Circ Res* 94:1533–1542.
63. del Monte F, Harding SE, Dec GW, Gwathmey JK, Hajjar RJ (2002) Targeting phospholamban by gene transfer in human heart failure. *Circulation* 105:904–907.
64. Hasenfuss G, Pieske B (2002) Calcium cycling in congestive heart failure. *J Mol Cell Cardiol* 34:951–969.
65. O'Rourke B, et al. (1999) Mechanisms of altered excitation-contraction coupling in canine tachycardia-induced heart failure, I: Experimental studies. *Circ Res* 84: 562–570.
66. Schmidt U, et al. (1998) Contribution of abnormal sarcoplasmic reticulum ATPase activity to systolic and diastolic dysfunction in human heart failure. *J Mol Cell Cardiol* 30:1929–1937.
67. Bick AG, Calvo SE, Mootha VK (2012) Evolutionary diversity of the mitochondrial calcium uniporter. *Science* 336:886.
68. Antony AN, et al. (2016) MICU1 regulation of mitochondrial Ca(2+) uptake dictates survival and tissue regeneration. *Nature Commun* 7:10955.
69. Liu JC, et al. (2016) Micu1 serves as a molecular gatekeeper to prevent in vivo mitochondrial calcium overload. *Cell Rep* 16:1561–1573.
70. Liu JC, et al. (2017) The in vivo biology of the mitochondrial calcium uniporter. *Mitochondrial Dynamics in Cardiovascular Medicine,* Advances in Experimental Medicine and Biology, ed Santulli G (Springer, Basinstoke, UK), Vol 982, pp 49–63.
71. Dong Z, et al. (2017) Mitochondrial Ca^{2+} uniporter is a mitochondrial luminal redox sensor that augments MCU channel activity. *Mol Cell* 65:1014–1028.e7.
72. Freestone T, et al. (1995) Inflammation and matrix metalloproteinases in the enlarging abdominal aortic aneurysm. *Arterioscler Thromb Vasc Biol* 15:1145–1151.
73. Newman KM, et al. (1994) Identification of matrix metalloproteinases 3 (stromelysin-1) and 9 (gelatinase B) in abdominal aortic aneurysm. *Arterioscler Thromb* 14: 1315–1320.
74. Ramos-Mozo P, et al. (2012) Plasma profiling by a protein array approach identifies IGFBP-1 as a novel biomarker of abdominal aortic aneurysm. *Atherosclerosis* 221: 544–550.
75. Shimizu K, Mitchell RN, Libby P (2006) Inflammation and cellular immune responses in abdominal aortic aneurysms. *Arterioscler Thromb Vasc Biol* 26:987–994.
76. Sukhanov S, et al. (2007) IGF-1 reduces inflammatory responses, suppresses oxidative stress, and decreases atherosclerosis progression in ApoE-deficient mice. *Arterioscler Thromb Vasc Biol* 27:2684–2690.
77. Palombo D, et al. (1999) Matrix metalloproteinases. Their role in degenerative chronic diseases of abdominal aorta. *J Cardiovasc Surg (Torino)* 40:257–260.
78. Morris DR, Biros E, Cronin O, Kuivaniemi H, Golledge J (2014) The association of genetic variants of matrix metalloproteinases with abdominal aortic aneurysm: A systematic review and meta-analysis. *Heart* 100:295–302.
79. Saracini C, et al. (2012) Polymorphisms of genes involved in extracellular matrix remodeling and abdominal aortic aneurysm. *J Vasc Surg* 55:171–179.e2.
80. Sasaki T, et al. (1987) Ehlers-Danlos syndrome. A variant characterized by the deficiency of pro alpha 2 chain of type I procollagen. *Arch Dermatol* 123:76–79.
81. Superti-Furga A, Gugler E, Gitzelmann R, Steinmann B (1988) Ehlers-Danlos syndrome type IV: A multi-exon deletion in one of the two COL3A1 alleles affecting

structure, stability, and processing of type III procollagen. *J Biol Chem* 263: 6226–6232.
82. Vissing H, et al. (1991) Multiexon deletion in the procollagen III gene is associated with mild Ehlers-Danlos syndrome type IV. *J Biol Chem* 266:5244–5248.
83. Boileau C, et al.; National Heart, Lung, and Blood Institute (NHLBI) GO Exome Sequencing Project (2012) TGFB2 mutations cause familial thoracic aortic aneurysms and dissections associated with mild systemic features of Marfan syndrome. *Nat Genet* 44:916–921.
84. Lerner-Ellis JP, et al. (2014) The spectrum of FBN1, TGFβR1, TGFβR2 and ACTA2 variants in 594 individuals with suspected Marfan syndrome, Loeys–Dietz syndrome or thoracic aortic aneurysms and dissections (TAAD). *Mol Genet Metab* 112:171–176.
85. Milewicz DM, et al. (1996) Fibrillin-1 (FBN1) mutations in patients with thoracic aortic aneurysms. *Circulation* 94:2708–2711.
86. Hofmann MA, et al. (1999) RAGE mediates a novel proinflammatory axis: A central cell surface receptor for S100/calgranulin polypeptides. *Cell* 97:889–901.
87. Averill MM, Kerkhoff C, Bornfeldt KE (2012) S100A8 and S100A9 in cardiovascular biology and disease. *Arterioscler Thromb Vasc Biol* 32:223–229.
88. Hofmann Bowman M, et al. (2010) S100A12 mediates aortic wall remodeling and aortic aneurysm. *Circ Res* 106:145–154.
89. Cao J, et al. (2013) Spatiotemporal expression of matrix metalloproteinases (MMPs) is regulated by the Ca^{2+}-signal transducer S100A4 in the pathogenesis of thoracic aortic aneurysm. *PLoS One* 8:e70057.
90. Coen M, et al. (2013) Smooth muscle cells of human intracranial aneurysms assume phenotypic features similar to those of the atherosclerotic plaque. *Cardiovasc Pathol* 22:339–344.
91. Olson ER, Shamhart PE, Naugle JE, Meszaros JG (2008) Angiotensin II-induced extracellular signal-regulated kinase 1/2 activation is mediated by protein kinase Cdelta and intracellular calcium in adult rat cardiac fibroblasts. *Hypertension* 51: 704–711.
92. Regalado ES, et al.; NHLBI GO Exome Sequencing Project (2011) Exome sequencing identifies SMAD3 mutations as a cause of familial thoracic aortic aneurysm and dissection with intracranial and other arterial aneurysms. *Circ Res* 109:680–686.
93. Shah BH, Catt KJ (2002) Calcium-independent activation of extracellularly regulated kinases 1 and 2 by angiotensin II in hepatic C9 cells: Roles of protein kinase Cdelta, Src/proline-rich tyrosine kinase 2, and epidermal growth receptor trans-activation. *Mol Pharmacol* 61:343–351.
94. Doyle JJ, et al. (2015) A deleterious gene-by-environment interaction imposed by calcium channel blockers in Marfan syndrome. *Elife* 4:e08648.
95. Wilmink AB, et al. (2002) Are antihypertensive drugs associated with abdominal aortic aneurysms? *J Vasc Surg* 36:751–757.
96. Doughan AK, Harrison DG, Dikalov SI (2008) Molecular mechanisms of angiotensin II-mediated mitochondrial dysfunction: Linking mitochondrial oxidative damage and vascular endothelial dysfunction. *Circ Res* 102:488–496.
97. Hoffman NE, et al. (2013) MICU1 motifs define mitochondrial calcium uniporter binding and activity. *Cell Rep* 5:1576–1588.
98. Daugherty A, Cassis LA (2004) Mouse models of abdominal aortic aneurysms. *Arterioscler Thromb Vasc Biol* 24:429–434.
99. Kuhlencordt PJ, et al. (2001) Accelerated atherosclerosis, aortic aneurysm formation, and ischemic heart disease in apolipoprotein E/endothelial nitric oxide synthase double-knockout mice. *Circulation* 104:448–454.
100. Choi S, et al. (2017) Mitochondrial calcium uniporter in *Drosophila* transfers calcium between the endoplasmic reticulum and mitochondria in oxidative stress-induced cell death. *J Biol Chem* 292:14473–14485.
101. Lim CC, Apstein CS, Colucci WS, Liao R (2000) Impaired cell shortening and relengthening with increased pacing frequency are intrinsic to the senescent mouse cardiomyocyte. *J Mol Cell Cardiol* 32:2075–2082.
102. Nagata K, et al. (1998) Early changes in excitation-contraction coupling: Transition from compensated hypertrophy to failure in Dahl salt-sensitive rat myocytes. *Cardiovasc Res* 37:467–477.
103. Zhan Y, et al. (2005) Ets-1 is a critical regulator of Ang II-mediated vascular inflammation and remodeling. *J Clin Invest* 115:2508–2516.
104. Chen PC, et al. (2010) Activation of multiple signaling pathways causes developmental defects in mice with a Noonan syndrome–associated *Sos1* mutation. *J Clin Invest* 120:4353–4365.
105. Christodoulou DC, Gorham JM, Herman DS, Seidman JG (2011) Construction of normalized RNA-seq libraries for next-generation sequencing using the crab duplex-specific nuclease. *Curr Protoc Mol Biol* 94:4.12.1–4.12.11.
106. Trombetta JJ, et al. (2014) Preparation of single-cell RNA-seq libraries for next generation sequencing. *Curr Protoc Mol Biol* 107:4.22.1–4.22.17.
107. Trapnell C, et al. (2012) Differential gene and transcript expression analysis of RNA-seq experiments with TopHat and Cufflinks. *Nat Protoc* 7:562–578.
108. Christodoulou DC, et al. (2011) Quantification of gene transcripts with deep sequencing analysis of gene expression (DSAGE) using 1 to 2 μg total RNA. *Curr Protoc Mol Biol* 93:25B.9.1–25B.9.16.
109. Trapnell C, et al. (2013) Differential analysis of gene regulation at transcript resolution with RNA-seq. *Nat Biotechnol* 31:46–53.
110. Burke MA, et al. (2014) Proliferation of cardiac fibroblasts defines early stages of genetic dilated cardiomyopathy and precedes myocardial metabolic derangement. *Circ Res* 115:A290.
111. Christodoulou DC, et al. (2014) 5′RNA-seq identifies Fhl1 as a genetic modifier in cardiomyopathy. *J Clin Invest* 124:1364–1370.
112. Huang W, Sherman BT, Lempicki RA (2009) Systematic and integrative analysis of large gene lists using DAVID bioinformatics resources. *Nat Protoc* 4:44–57.
113. Wu AR, et al. (2014) Quantitative assessment of single-cell RNA-sequencing methods. *Nat Methods* 11:41–46.